Food Research International 222 (2025) 117802

Contents lists available at ScienceDirect

Food Research International

journal homepage: www.elsevier.com/locate/foodres

Thermophysical properties of eutectic mixtures composed by oleic acid and components of essential oils

Elena Pérez-Pueyo [a], Héctor Artigas [a,b], Mohammadreza Haftbaradaran Esfahani [a], Carlos Lafuente [a,b], Manuela Artal [a,*]

[a] Departamento de Química Física, Facultad de Ciencias, Universidad de Zaragoza, Zaragoza, Spain
[b] Instituto Agroalimentario de Aragón - IA2 (Universidad de Zaragoza - CITA), Zaragoza, Spain

ARTICLE INFO

Keywords:
Oleic acid
Essential oils
Hydrophobic eutectic solvents
Thermodynamic and transport properties

ABSTRACT

Currently, replacing traditional solvents with others whose components are considered safe is one of the most important challenges in the chemical industry. However, this change cannot be achieved without understanding the behavior of fluids under different operating conditions. To achieve this, thermophysical properties must be either determined experimentally over wide ranges of pressure, temperature, and composition, or tools must be available to predict them. Here, we studied binary mixtures of Generally Recognize as Safe (GRAS) compounds. These mixtures could be used both as extractants of natural products and solvents of poorly-water soluble ones. Specifically, they are oleic acid-based systems with thymol, l-menthol, eugenol, or linalool. The measured properties were the phase change equilibria, density, speed of sound, refractive index, isobaric molar heat capacity, surface tension, and kinematic viscosity at 0.1 MPa and from 283.15 to 338.15 K. In addition, several derived properties were calculated, different correlations were used and the PC-SAFT equation of state (EoS) was validated. All mixtures were less dense than water and moderately viscous. The most and least compact mixtures were those with eugenol and linalool, respectively. The prediction of the isobaric molar heat capacity from both molar mass and critical properties, as well as EoS, showed a deviation of less than 5 % from the measured values. For the density, the maximum mean relative deviation with the EoS results was of 0.19 %.

1. Introduction

Growing consumer concern about environmental issues has exponentially increased interest in compounds extracted from natural sources. At the same time, these processes require a high level of sustainability. It is known that one of the most problematic steps in terms of energy costs and waste generation is the separation and recycling of the solvent (Ferreira & Sarraguça, 2024; Isci & Kaltschmitt, 2022). One proposal that avoids this step and, at the same time, improves the properties of the final product is to use natural deep eutectic solvents (NADES). They are mixtures of compounds that are usually obtained from matrices of natural origin as primary metabolites, among others. The difference between the inter- and intra-components interactions, and the entropic effect resulting from the mixing process, means that their fusion temperature (T_f) is much lower than it would be if the mixture behaved ideally. Therefore, they are liquids over a wide temperature range. Furthermore, they have been shown to be good solvents even for solutes with low soluble content in aqueous solutions because the network of interactions gives them an affinity for many compounds (Bergua, Delso, et al., 2021; Padilla et al., 2024). Depending on their behavior towards water, NADESs can have a hydrophilic or hydrophobic character. In the first, a supramolecular structure is formed, resulting in a significant decrease in T_f (Delso et al., 2019). In most of the latter, hydrophobic interactions predominate so the T_f depression is small, and the qualifier "*deep*" should not be used. They are simply referred to as hydrophobic eutectic solvents (hESs) and are especially interesting in two-phase separation and extraction processes (Bergua, Castro, et al., 2021; Bergua, Castro, Lafuente, & Artal, 2022; Bergua, Castro, Muñoz-Embid, et al., 2022). More information on the origin, preparation, properties, and uses of the eutectic solvents can be found in the literature (del Mar Contreras-Gámez et al., 2023; Liu et al., 2018; Martins, Crespo, et al., 2018; Paiva et al., 2014; Sportiello et al., 2023; Tapia-Quirós et al., 2024; Van Osch et al., 2015; Yan et al., 2025; Zhang et al., 2023). Note that not removing the eutectic mixture used as

* Corresponding author.
E-mail address: martal@unizar.es (M. Artal).

https://doi.org/10.1016/j.foodres.2025.117802
Received 20 May 2025; Received in revised form 27 October 2025; Accepted 30 October 2025
Available online 1 November 2025

a solvent in the extraction of a bioactive compound can have a positive effect on the final formulation of the active ingredient. For example, it can increase its antioxidant capacity, antimicrobial activity or transdermal penetrability by synergistic effect with the components of the mixture (Abdelquader et al., 2023; Artigas-Hernández et al., 2023; Chen et al., 2025; Marañés et al., 2025; Mussagy et al., 2023; Mussagy, Remonatto, et al., 2022; Mussagy, Santos-Ebinuma, et al., 2022). Taking this into account, we have chosen to study binary mixtures of oleic acid (Oa) and different components of essential oils as thymol (5-Methyl-2-(propan-2-il)phenol) (T), l-menthol (5-Methyl-2-(propan-2-yl)cyclohexan-1-ol) (M), eugenol (4-Allyl-2-methoxyphenol) (E), and linalool (2,6-dimethyl-2,7-octadien-6-ol) (L). The Oa belongs to the group of omega-9 fatty acids, monounsaturated acids with the double bond in the 9th position. It can be obtained from both plant sources (mainly olives and camellia), animal sources (livestock and fish), and to a much lesser extent, microbial sources. The health benefits of including it in the diet are well-known. It prevents cardiovascular disease and nervous system degeneration, is a powerful antioxidant, and reduces the body's inflammatory response that can lead to cancer or diabetes (Wang et al., 2024). Also, it is an efficient plasticizer so its use in new and more sustainable packaging systems is being evaluated (Vlacha et al., 2016). Regarding the second components of binary mixtures, T and M are monoterpenes that differ only in the type of ring contained in their structure. Both are extracted from plants (thyme and menthe families) and are used in the cosmetic, agri-food, and pharmaceutical industries. They promote transdermal penetrability and have different therapeutic properties (Zielińska-Błajet et al., 2021). Moreover, the E is a phenylpropanoid mainly extracted from the essential oils of the cloves and cinnamon. Its traditional application has been the formation of dental cement by adding zinc oxide. Currently, its potential has been seen both in pharmacology and in the agri-food industry as a food preservative (Khwaza & Aderibigbe, 2025). The L is an acyclic monoterpene alcohol present in plants such as cinnamon, coriander, and lavender. It has a pleasant floral aroma, so it is used in perfumes, cleaners, and cosmetic products. It is also used as an additive in processed foods and beverages, as a natural preservative and food flavoring. Its bioactive properties include high anticancer, antifungal and antibacterial activity, protecting liver, kidney and lung functions (An et al., 2021). Synergistic effects have been observed when using mixtures of Oa and terpenes to improve the efficiency of extraction processes, and the antioxidant, antimycobacterial and antifungal capacities of a compound (Artigas-Hernández et al., 2023; Mussagy et al., 2023; Pitacco et al., 2022; Radwan et al., 2024; Sieniawska et al., 2017). Despite this, there is hardly any published data on the properties of these mixtures. Duque et al. (Duque et al., 2023) characterized two mixtures of T and Oa but the compositions did not match ours. Ion et al. (Ion et al., 2022) measured solid-liquid phase change temperatures of three mixtures of M and Oa including the MOa composition. In addition, the refractive index of two of them (no MOa) was determined. Recently, our group measured the properties of the four mixtures at 298.15 K (Marañés et al., 2025).

This work focuses on assessing the thermophysical behavior of four hydrophobic systems. They are binary mixtures of oleic acid and thymol, l-menthol, eugenol, or linalool. The article is organized as follows. First, the preparation and characteristics of the studied mixtures and used devices are explained. It continues with a section that includes a brief description of the models and correlations subsequently used in the discussion of the results. The final section presents and analyzes the experimental data of the phase change, density, speed of sound, refractive index, isobaric molar heat capacity, surface tension, and kinematic viscosity at 0.1 MPa and from 283.15 K to 338.15 K.

2. Materials and methods

2.1. Chemicals

The chemicals used to prepare the oleic acid-based eutectic solvents (Oa ESs) and their acronyms were oleic acid (Oa), thymol (T), l-menthol (M), eugenol (E), and linalool (L). No purification processes were applied after the commercial supply. The characteristics and structures of these compounds are reported in Table S1 (supplementary material).

2.2. Preparation of oleic acid-based eutectic mixtures

Four mixtures containing Oa and a component of essential oil were prepared. The compositions were equimolar except for the mixture with T since it was solid at 298 K. In this case, the composition of the mixture, in mole fraction of oleic acid, was x_{Oa}=0.6. To prepare the samples, appropriate amounts of each component of the binary mixture were weighed in a flask with a Sartorius PB210S balance ($u(m)$=1·10^{-4} g). Subsequently, simultaneous stirring and gentle heating (323*K*) were carried out until the liquid mixture was homogeneous. The mixtures were cooled slowly and no crystallization was observed in any sample. In addition, no decomposition or reaction was observed in the mixing process of Oa ESs, as can be concluded from the NMR spectra collected in Fig. S1. In them, all peaks detected for the pure components of each mixture are also found in the corresponding Oa ES. No additional peaks were observed. The Karl-Fischer method (automatic titrator Crison KF 1S—2B) was used to measure the water content. Table 1 lists a description of the Oa ESs studied in this work and a picture is found in the Supplementary File.

2.3. Phase change

A differential scanning calorimeter (TA Instruments DSC Q2000) equipped with an RCS cooling system was used to determine the phase change temperatures and enthalpies. A sample of Indium was used as standard compound to calibrate the apparatus. The uncertainties were calculated from the differences between the expected values and those from the calibration. The values were $u(T)$=0.5 K and $u(\Delta H)$=1 kJ/mol. In each measurement, an aluminum dish was filled with a mass between 5 and 10 mg of sample. It was cooled to 213 K and then heated to 318 K at a rate of 3 K/min.

2.4. Thermophysical characterization

The thermophysical properties were measured with different devices frequently described in the literature. In Table 2, we only summarize their characteristics: the type of apparatus, uncertainties in the measurements, several details of the procedures, and the validation of each apparatus. The latter was carried out by comparison between experimental and literature data for standard fluids (Antón et al., 2017; López et al., 2020).

3. Theory

3.1. PcC-SAFT

In this section, a brief description of this equation of state (EoS) is presented. The reader can find further information on in the papers published by Gross and Sadowski (Gross & Sadowski, 2000, 2001). The model describes the Helmholtz energy ($\tilde{a}$) as the sum of several terms: the contribution of ideal gas ($\tilde{a}^{id}$), the repulsive term represented by the hard-chain reference system ($\tilde{a}^{hc}$), and the attractive terms of dispersive ($\tilde{a}^{dis}$) and association ($\tilde{a}^{assoc}$) interactions. The equations are:

$$\tilde{a} = \tilde{a}^{id} + \tilde{a}^{hc} + \tilde{a}^{dis} + \tilde{a}^{assoc} \quad (1)$$

$$\tilde{a}^{hc} = m\tilde{a}^{hs} - (m-1)\ln g^{hs} \quad (2)$$

Table 1
Description of the oleic acid-based eutectic solvents (Oa ESs): Acronym, mole fraction in oleic acid (x_{Oa}), molar mass calculated ($M_{Oa\ ES}$)[a], and appearance at $T = 298.15$ K and $p = 0.1$ MPa.

Oa ES acronym	Compound 1 (acronym)	Compound 2 (acronym)	x_{Oa}	$M_{Oa\ ES}$/ (g/mol)	Water content(ppm)	Appearance
T3Oa5	Thymol (T)	Oleic acid (Oa)	0.6	229.56	244	colorless liquid
MOa	l-menthol (M)	Oleic acid (Oa)	0.5	219.37	220	colorless liquid
EOa	Eugenol (E)	Oleic acid (Oa)	0.5	223.33	283	orange liquid
LOa	Linalool (L)	Oleic acid (Oa)	0.5	218.36	260	colorless liquid

[a] $M_{Oa\ ES} = \sum_i M_i x_i$,

Table 2
Overview of the apparatus used to measure the thermophysical properties.

Property	Devices	$u(T)$/K	$U_c(Y)$[a]	$MRD(Y)$[b]/%
Density, ρ	Oscillating U-tube density meter, Anton Paar DSA 5000 [c]	0.005	0.05 kg/m^3	0.004
Speed of sound, u	Sing-around technique in a fixed-path interferometer, Anton Paar DSA 5000 [c]	0.005	0.5 m/s	0.026
Isobaric molar heat capacity, $C_{p,m}$	Differential scanning calorimeter, TA Instruments DSC Q2000 [d]	0.5	1 %	0.028
Refractive index, n_D	Standard Abbe refractometer, Abbemat-HP refractometer Dr. Kernchen [e]	0.01	$2{\cdot}10^{-5}$	0.007
Surface tension, γ	Drop volume tensiometer, Lauda TVT-2 [e,f]	0.01	1 %	0.21
Kinematic viscosity, ν	Capillary viscosimeter Ubbelohde, Schoot-Geräte AVS-440	0.01	1 %	0.28

[a] $k = 2$ (0.95 level of confidence); [b] $MRD(Y) = \frac{100}{n}\sum_{i=1}^{n}\left|\frac{Y_{i,lit} - Y_{i,exp}}{Y_{i,exp}}\right|$; [c] Calibrated with two reference fluids: air and water MilliQ (resistivity of 18.2 μS/cm); [d] Synthetic sapphire was used as standard reference; [e] Calibrated with water MilliQ (resistivity of 18.2 μS/cm) as reference fluid; [f] 16 drops were averaged

$$\tilde{a}^{\mathrm{dis}} = -2\pi\rho m^2\left(\frac{\varepsilon}{kT}\right)\sigma^3\sum_{i=0}^{6}\left[a_{0i} + \frac{m-1}{m}a_{1i} + \frac{m-1}{m}\frac{m-2}{m}a_{2i}\right]\eta^i - \pi\rho mkT\left(\frac{\partial\rho}{\partial p}\right)_{hc} m^2\left(\frac{\varepsilon}{kT}\right)^2\sigma^3\sum_{i=0}^{6}\left[b_{0i} + \frac{m-1}{m}b_{1i} + \frac{m-1}{m}\frac{m-2}{m}b_{2i}\right]\eta^i \quad (3)$$

$$\tilde{a}^{\mathrm{assoc}} = \sum_A\left[\ln\left(1+\rho X^A\Delta\right)^{-1} - \frac{\left(1+\rho X^A\Delta\right)^{-1}}{2}\right] + \frac{1}{2}S \quad (4)$$

$$\Delta = \kappa^{A_iB_i}\sigma^3 g^{hs}\left[\exp\left(\frac{\varepsilon^{A_iB_i}}{kT}\right) - 1\right] \quad (5)$$

where $a_{0i}, a_{1i}, a_{2i}, b_{0i}, b_{1i}$, and b_{2i}, are called *universal constants* and their values were obtained from the thermodynamic properties of *n*-alkanes. Also, m is the chain segment number, g^{hs} is the radial pair distribution function of the segments, $\tilde{a}^{\mathrm{hs}}$ is the Helmholtz energy of the hard sphere, ρ is the density, p is the pressure, T is the temperature, σ is the segment diameter, ε is the segment energy, η is the packing fraction, X^A is the fraction of unbonded monomers, Δ is the tendency to form *n*-mers, $\kappa^{A_iB_i}$ is the association volume, $\varepsilon^{A_iB_i}$ is the association energy, and S is the number of associated sites of the compound. Therefore, 3 geometric parameters (m, σ and ε), two association parameters ($\kappa^{A_iB_i}$ and $\varepsilon^{A_iB_i}$), and an association scheme are needed to characterize each pure compound capable of associating. They are usually calculated from data of thermodynamic properties of the pure compounds. Table 3 summarizes the parameters used in this work.

The mixing rules used to model our systems were:

$$\sigma_{ij} = (\sigma_i + \sigma_j)/2 \quad (6)$$

$$\varepsilon_{ij} = \sqrt{\varepsilon_i\varepsilon_j}(1 - k_{ij}) \quad (7)$$

$$\kappa^{A_iB_j} = \sqrt{\kappa^{A_iB_i}\ \kappa^{A_jB_j}} \quad (8)$$

$$\varepsilon^{A_iB_j} = \left(\varepsilon^{A_iB_i} + \varepsilon^{A_jB_j}\right)/2 \quad (9)$$

where the subscripts i and j refer to each of the compounds present in the mixture, and k_{ij} is the binary interaction parameter. We used the model in its predictive version (k_{ij}=0) for all mixtures. To improve the estimated density of the LOa mixture, calculations were performed for this ES with an optimized parameter, $k_{ij} = -0.05$.

3.2. Estimation of the isobaric molar heat capacity

The $C_{p,m}$ of mixtures can be estimate from critical properties with the correlation of Taherzadeh et al. (Taherzadeh et al., 2020):

$$C_{p,m} = A + 132.27\ T^{1/4}, \quad (10)$$

$$A = 3.8 \bullet 10^{-4}\frac{M_{Oa\ ES}^3}{p_c^6} + 6.3 \bullet 10^{-5}M_{Oa\ ESs}^{2\omega} - \frac{24577.4}{M_{Oa\ ES}} - 94.9, \quad (11)$$

where T is the temperature, $M_{Oa\ ES}$ is the molar mass (Table 1), p_c is the critical pressure, and ω is the acentric factor of each mixture. The last two parameters were estimated from the Lee-Kesler (LK) mixing rules:

Table 3
Parameters of the pure compounds in the modelling of the oleic acid-based ESs (Oa ESs) with the PC-SAFT EoS. The type 2B (one donor and one acceptor site) was considered as association scheme.

Compound	m/M	σ/ Å	ε/ K	$\kappa^{A_iB_i}$	$\varepsilon^{A_iB_i}$ / K	Reference
Oleic acid	0.03090	3.712	254.78	0.0183	810.92	(dos Santos et al., 2017)
Thymol	0.02671	3.816	290.22	0.0616	1660	(Martins, Crespo, et al., 2018)
l-Menthol	0.02657	3.903	262.40	0.0996	1785.6	(Martins, Crespo, et al., 2018)
Eugenol	0.02696	3.698	290.00	0.0616	1660	This work
Linalool	0.02721	3.919	271.74	0.0019	2187.3	(Torcal et al., 2010)

$$p_c(\text{bar}) = (0.2905 - 0.0850\omega)\frac{83.1447T_c}{V_c}, \tag{12}$$

$$\omega = \sum_{n=1}^{3} x_n\omega_n, \tag{13}$$

$$V_c(\text{mL/mol}) = \sum_{n=1}^{3}\sum_{m=1}^{3} x_n x_m V_{c,mn}, \tag{14}$$

$$T_c(\text{K}) = \frac{1}{V_c^{0.25}}\sum_{n=1}^{3}\sum_{m=1}^{3} x_n x_m V_{c,mn}^{0.25} T_{c,mn}, \tag{15}$$

$$V_{c,mn}(\text{mL/mol}) = \frac{1}{8}\left(V_{c,n}^{1/3} + V_{c,m}^{1/3}\right)^3, \tag{16}$$

$$T_{c,mn}(\text{K}) = \left(T_{c,n}T_{c,m}\right)^{0.5}, \tag{17}$$

where the subscripts n and m represent each component, and mn is the subscript indicating binary interaction term. T_c and V_c are the critical temperature and critical volume of the Oa ES.

3.3. Estimation of the critical temperature

The T_c of our Oa ESs were calculated with PC-SAFT EoS (eq. 1–9) and the LK mixing rules (eq. 12–17). In addition, the equations of Guggenheim (Guggenheim, 1945) and Eötvos (Shereshefsky, 1930) were used:

$$\gamma = \gamma_0(1 - T/T_c)^{11/9}, \tag{18}$$

$$\gamma(M_{Oa\ ESs}/\rho)^{2/3} = K(T_c - T), \tag{19}$$

where γ_0 is the surface tension at 0 K, $M_{Oa\ ESs}$ is the molar mass of the Oa ESs (Table 1), and γ and ρ are the surface tension and density at the temperature T.

3.4. Estimation of the surface tension

The equation of Papazian (Papazian, 1971) correlates γ and n_D, as follows:

$$\gamma = A\left(\frac{n_D^2 - 1}{2n_D^2 + 1}\right) + B, \tag{20}$$

where A, and B are the fit coefficients. Furthermore, the equations of Pelofsky and Murkerjee (Pelofsky, 1966) correlate γ and η:

$$\ln\gamma = \ln A_1 + \frac{B_1}{\eta}, \tag{21}$$

$$\ln\gamma = \ln A_2 + \frac{B_2}{3}\ln\eta, \tag{22}$$

where, A_1, A_2, B_1, and B_2 are the fit coefficients.

4. Results

4.1. Phase change

Data corresponding to the phase transitions of the Oa ESs studied are collected in Table 4. The thermograms from which this information was obtained are found in the supplementary file. In the T3Oa5 mixture, three exothermic and two endothermic events were observed (Fig. S2a). The first exothermic peak corresponded to crystallization of a metastable α-phase, typically reported around 272 K in pure Oa (García-Zapateiro et al., 2013). Thymol lowers this temperature by donating hydrogen bonds, disrupting lattice packing, and stabilizing the liquid state (Abranches et al., 2019; Pour et al., 2022). A subsequent α → γ polymorphic transformation occurs near 262.15 K (García-Zapateiro et al., 2013), followed by a reversible γ → α transition at ~268 K (Tandon et al., 2000). Recrystallization gave rise to the final exothermic event, while the last endothermic peak corresponded to melting. The MOa mixture displayed two exothermic peaks, associated with α-phase crystallization and α → γ transformation of Oa, along with two broad endothermic signals (γ → α transition and glass transition) and two sharper peaks attributed to eutectic formation (Fig. S2b). The presence of multiple eutectic events reflected the polymorphic complexity of M, with transitions around 268 K coinciding with the reported β → α transformation in pure M (Corvis & Espeau, 2012; Štejfa et al., 2019). The EOa thermogram showed two exothermic and two endothermic transitions, with only partial recrystallization (Fig. S2c). For the LOa system, two exothermic peaks (α-phase crystallization and α → γ transition), and three endothermic peaks (γ → α transition in Oa, and two poorly defined eutectic events) were observed (Fig. S2d). The more negative the difference between the melting point of a mixture and that considered ideal behavior, the greater its eutectic character (Martins, Pinho, et al., 2018). In our mixtures, T3Oa5 and MOa were slightly eutectic, while EOa and LOa were ideal.

4.2. Thermophysical characterization

In this section, results of five thermodynamic and one transport properties of four Oa ESs are presented and discussed. All properties were measured at 0.1 MPa and at temperatures from 283.15 K to 338.15 K in intervals of 2.5 K. The selected temperature range is a result of combining two criteria: the minimum temperature at which the mixture is liquid, and the temperature range for which the devices can adequately measure. Measurements were taken every 2.5 K to accurately calculate the derived properties. The values are reported in the supplementary file (Tables S2-S7). Also, Table 5 lists data of the properties at 293.15 K to easier the reader of this section. No literature data were found to compare with our results for any of the measured properties of our mixtures. However, the values obtained in this work of ρ, n_D, γ, and η at 298.15 K can be compared with those found in the literature for the mixtures with decanoic acid (Bergua, Castro, et al., 2021; Bergua, Castro, Muñoz-Embid, et al., 2022; Patra et al., 2022).

Table 4
Properties of phase change of the Oa ESs characterized. Temperature ($T_{\alpha\to\gamma}$) and enthalpy ($\Delta H_{\alpha\to\gamma}$) of the α → γ polymorphic transformation of Oa, temperature ($T_{\gamma\to\alpha}$) and enthalpy ($\Delta H_{\gamma\to\alpha}$) of the γ → α polymorphic transformation of Oa, temperature ($T_{cr,\alpha}$) and enthalpy ($\Delta H_{cr,\alpha}$) of the crystallization of metastable α phase, and melting temperature (T_m) and enthalpy (ΔH_m).

Oa ESs	$T_{\alpha\to\gamma}$/ K	$T_{\gamma\to\alpha}$ / K	$T_{cr,\alpha}$ / K	T_m/ K	$\Delta H_{\alpha\to\gamma}$/ kJ/mol	$\Delta H_{\gamma\to\alpha}$/ kJ/mol	$\Delta H_{cr,\alpha}$/ kJ/mol	ΔH_m/ kJ/mol
T3Oa5	257.33	262.04	270.90	278.11/286[a]	1.816	2.005	8.899	12.261
MOa	253.52	258.90	262.93	272.47/277[a]	2.120	0.174	5.455	1.907
EOa	255.52	260.80	268.70	276.82/276[a]	1.449	1.352	8.429	7.211
LOa	257.42	261.01	272.15	271.71/271[a]	0.212	0.197	3.509	0.446

[a] T_m considered ideal behavior; calculated from Schraeder equation (Prausnitz et al., 1986).

Table 5
Summary of the thermophysical properties[a] of the Oa ESs studied at T = 293.15 K and p = 0.1 MPa.

Property	T3Oa5[b]	MOa[c]	EOa[d]	LOa[e]
Density, ρ/(kg/m^3)	912.22	894.60	948.29	888.76
Speed of sound, u/(m/s)	1438.95	1421.60	1445.15	1404.93
Refraction index, n_D	1.47612	1.46160	1.48629	1.46152
Isobaric molar heat capacity, $C_{p,m}$/(J/mol·K)	502	465	474	473
Surface tension, γ/(mN/m)	31.95	31.01	32.71	30.02
Dynamic viscosity, η/(mPa·s)	32.66	38.73	23.06	20.80
Isobaric expansibility, α_p/(kK^{-1})	0.783	0.781	0.799	0.824
Isentropic compressibility, κ_s/(TPa^{-1})	535.83	553.12	504.94	570.04
Free intermolecular length, L_f/Å	0.453	0.461	0.440	0.468
Molar refraction, R_m/ (cm^3/mol)	70.99	67.36	67.65	67.48
Free volume, f_m/ (cm^3/mol)	180.66	177.85	167.86	178.21
Joule-Thomson coefficient, μ_{JT}/ (K/MPa)	−0.386	−0.406	−0.381	−0.394
Entropy of surface, ΔS_S/(mN/m·K)	0.0724	0.0771	0.0737	0.0819
Enthalpy of surface, ΔH_S/(mN/m)	53.17	53.61	54.32	54.03
Activation energy of viscous flow, $E_{a,\eta}$/(kJ/mol)	32.98	38.01	31.60	30.62

[a] Standard uncertainties are: $u(T)$=0.005 K for density and speed of sound and 0.01 K for the rest of properties; $u(p)$=0.5 kPa. The combined expanded uncertainties (0.95 level of confidence, k=2) are $U_c(\rho)$=0.05 kg/m^3; $U_c(u)$=0.5 m/s; $U_c(n_D)$=2·10^{-5}; $U_c(C_{p,m})$=1 %; $U_c(\gamma)$=1 %; $U_c(\eta)$=1 %; $U_c(\alpha_p)$=0.04 kK^{-1}; $U_c(\kappa_s)$=0.30 TPa^{-1}; $U_c(L_f)$=0.005 Å; $U_c(R_m)$=0.007 cm^3/mol; $U_c(f_m)$=0.05 cm^3/mol; $U_c(\Delta S_S)$=0.001 mN/m·K; $U_c(\Delta H_S)$=0.06 mN/m. [b] Thymol:oleic acid, x_{Oa}=0.6; [c] l-menthol:oleic acid, x_{Oa}=0.5; [d] eugenol:oleic acid, x_{Oa}=0.5; [e] linalool:oleic acid, x_{Oa}=0.5.

4.2.1. Density

The ρ values of all studied Oa ESs (Table S2) were lower than those of the water and these differences were higher than 50 kg/m^3. So, these hydrophobic mixtures could be suitable to use in liquid-liquid extractions. The sequence of density in the range of temperatures studied was LOa < MOa < T3Oa5 < EOa. The eutectics formed by the acyclic compound (L) were the least dense mixtures. On the other hand, the densest Oa ESs were those containing phenols in which the presence of the aromatic ring provides a flatter structure. Finally, the density of the mixture with M, a non-aromatic cyclic compound, had an intermediate value. The ρ sequence was similar to that found for the mixtures of these compounds with decanoic acid. Changing decanoic acid to oleic acid in the mixture with L increased the density by 1 %. In contrast, the density of the mixture with E was approximately 2 % lower, and was barely affected in the mixtures with T and M. The less planar structures favored greater interaction with the Oa chain. Having a tool that allows estimating the thermodynamic behavior of a fluid is essential in the operational design of industrial processes. Equations of state as PC-SAFT model (section 3.1) have traditionally been used for this purpose; however, they must be previously validated for each system. Here, we predicted the densities of our Oa ESs with this EoS and compared the values with those determined experimentally. Except for LOa, the predicted values coincided with the measured ones and for that one, the deviation decreased markedly when considering a non-zero binary interaction parameter (Table 6). A graphical comparison is presented in Fig. S3a and S3b.

The increase in temperature decreases the intermolecular forces so the density also decreases (Fig. 1a). In liquids, this correlation is usually a linear equation. For our systems, the coefficients are found in Table 7. The volumetric behavior of fluids with temperature is an important property in the operational design of processes. To quantify this, the isobaric expansion coefficient was calculated as $\alpha_p = (-\ \partial \ln\rho/\partial T)_p$. Table 5 lists the values at 293.15 K and Fig. 1b shows the calculated ones at all temperatures. They increased with T and the temperature coefficients ($\partial\alpha_p/\partial T$) ranged from 6.25·10^{-4} kK^{-2} for MOa to 7.00·10^{-4} kK^{-2} for LOa.

Table 6
Mean relative deviations[a] in the modelling of Oa ESs with the PC-SAFT EoS.

Oa ESs	k_{ij}	$MRD(\rho)$/%	$MRD(u)$/%	$MRD(C_{p,m})$/%	$MRD(\mu_{JT})$/%
T3Oa5[b]	0	0.17	18	2.64	2.22
MOa[c]	0	0.18	19	4.41	2.70
EOa[d]	0	0.16	17	1.96	2.00
LOa[e]	0	0.96	18	4.15	1.27
	−0.05	0.19	16	3.25	1.39

[a] $MRD(Y) = \frac{100}{n}\sum_{i=1}^{n}\left|\frac{Y_{i,PC-SAFT} - Y_{i,exp}}{Y_{i,exp}}\right|$, [b] Thymol:oleic acid, x_{Oa}=0.6; [c] l-menthol:oleic acid, x_{Oa}=0.5; [d] eugenol:oleic acid, x_{Oa}=0.5; [e] linalool:oleic acid, x_{Oa}=0.5.

4.2.2. Speed of sound

The speed of sound propagation through a material is greater the more compact the material is. According to the determined u values (Table S3, Table 5), the compaction order matched with that found for ρ, LOa < MOa < T3Oa5 < EOa. Regarding the prediction of the u with PC-SAFT (section 3.1), the model is not adequate as shown in Table 6. The increase in thermal energy makes it difficult to compact the liquid, so the linear $u - T$ relationship has a negative slope (Table 7, Fig. 2a). From ρ and u data under the same conditions, the isentropic compressibility ($\kappa_S = 1/(\rho u^2)$) was calculated. This property indicates the compression capacity of a fluid while maintaining constant entropy. As expected, the values followed a sequence opposite to that found for u. Fig. 2b displays the variation of κ_S with T, that is more pronounced for the less compact mixtures as shown by the temperature coefficients ($\partial\kappa_S/\partial T$). They ranged from 3.292 TPa^{-1}·K^{-1} for EOa to 3.813 TPa^{-1}·K^{-1} for LOa. From its definition, it is deduced that κ_S is related to the free intermolecular length (L_f). An estimation was proposed by Jacobson (Jacobson, 1952) as $L_f = K\sqrt{\kappa_S}$. Table 5 lists the values at 293.15 K, which were 0.1 Å smaller than those at 338.15 K.

4.2.3. Refractive index

The more compact a fluid is, the slower the speed of light travels. The n_D is defined as the ratio of the apparent speed of light in the vacuum to the speed in the medium measured at the yellow doublet D-line of sodium (589 nm). Therefore, more compact fluids have higher n_D values. The results listed in Tables 5 and S4 were in agreement with those obtained in the previous section. The n_D values of our mixtures were higher than those obtained in the corresponding ones with decanoic acid. Fig. 3a shows the linear decrease of n_D with T as a result of increasing thermal agitation. The coefficients are reported in Table 7. The molar refraction (R_m) is related to the polarizability of a mole of substance and is calculated from molar volume ($V_m = M/\rho$) and n_D data with the Lorentz-Lorentz equation:

$$R_m = V_m \frac{(n_D^2 - 1)}{(n_D^2 + 2)} \tag{23}$$

The mixture with T had the highest R_m and the rest showed similar values (Table 5). They increased with T in a similar way (Fig. 3b) and the average temperature coefficient ($\partial R_m/\partial T$) was (4.0 ± 0.3)·10^{-3} cm^3/mol·K. The free intermolecular volume (f_m) can be calculated by subtraction between V_m and R_m owing the latter is related to the volume occupied by a mole of hard cores of the molecules (Brocos et al., 2003). The sequence of values obtained was EOa < MOa < LOa < T3Oa5 (Table 5). Considering the V_m of each Oa ES, the sequence of the free volume percentage at 293.15 K was EOa (71.3 %) < T3Oa5 (71.8 %) < MOa (72.5 %) = LOa (72.5 %). These values increased by 1 % to 338.15 K.

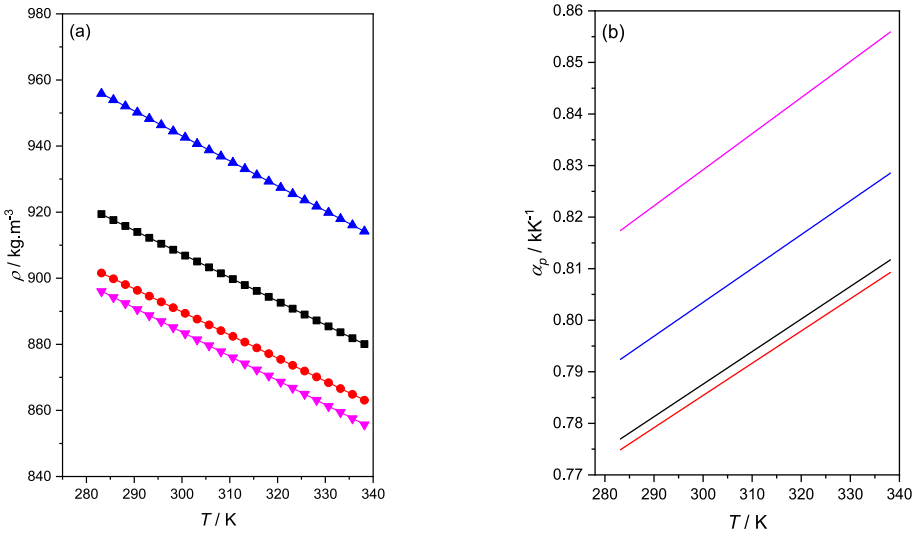

Fig. 1. Properties of oleic acid-based ESs at p=0.1 MPa at various temperatures (T) and compositions. (a), Density (ρ); (b) Isobaric thermal expansion coefficient (α_p). (■), Thymol:oleic acid, x_{Oa}=0.6; (●), l-menthol:oleic acid, x_{Oa}=0.5; (▲), eugenol:oleic acid, x_{Oa}=0.5; (▼), linalool:oleic acid, x_{Oa}=0.5. Points, experimental values; lines, calculated data.

Table 7
Correlation of each thermodynamical property with temperature [a] of the Oa ESs studied. Fitting parameters (A_Y, B_Y) and regression coefficients (R^2).

Property	Oa ESs	A_Y	B_Y	R^2
Density, ρ /(kg/m^3)	T3Oa5[b]	1127.72	−0.7146	1
	MOa[c]	1099.46	−0.6988	1
	EOa[d]	1170.37	−0.7576	1
	LOa[e]	1103.55	−0.7327	1
Speed of sound, u /(m/s)	T3Oa5[b]	2428.70	−3.3771	0.9998
	MOa[c]	2394.65	−3.3208	0.9983
	EOa[d]	2469.38	−3.4937	1
	LOa[e]	2421.51	−3.4671	1
Refractive index, n_D	T3Oa5[b]	1.59386	$-4.02\cdot10^{-4}$	1
	MOa[c]	1.57594	$-3.88\cdot10^{-4}$	1
	EOa[d]	1.60900	$-4.18\cdot10^{-4}$	0.9999
	LOa[e]	1.58145	$-4.09\cdot10^{-4}$	1
Isobaric molar heat capacity, $C_{p,m}$/(J/mol·K)	T3Oa5[b]	231.31	0.9232	0.9999
	MOa[c]	72.932	1.3387	1
	EOa[d]	284.49	0.6455	0.9999
	LOa[e]	196.77	0.9428	0.9999
Surface tension, γ/(mN/m)	T3Oa5[b]	53.16	−0.0724	0.9973
	MOa[c]	53.60	−0.0771	0.9991
	EOa[d]	54.40	−0.0737	0.9990
	LOa[e]	54.02	−0.0819	0.9995

[a] $Y = A_Y + B_Y T$, [b] Thymol:oleic acid, x_{Oa}=0.6; [c] l-menthol:oleic acid, x_{Oa}=0.5; [d] eugenol:oleic acid, x_{Oa}=0.5; [e] linalool:oleic acid, x_{Oa}=0.5.

4.2.4. Isobaric molar heat capacity

The $C_{p,m}$ is defined as the amount of heat that must be supplied to one mole of substance to increase its temperature by one kelvin at constant pressure. It depends on three factors: the molar mass, internal degrees of freedom, and hydrogen bonds. The first two factors are greater, especially the second, in the T3Oa5 mixture than in the others, due to the higher Oa ratio. In our mixtures, the order of molar masses was the inverse of that of degrees of freedom in L, M, and E. Regarding the last factor, E has a greater capacity to form hydrogen bonds (1 HBD and 2 HBA) than T, M, and L (1 HBD and 1 HBA) but maintaining them become more difficult as T increase. All of this could explain the $C_{p,m}$ values measured (Tables 5 and S5). This property was greater in the T3Oa5 mixture, and changes in trend with T were observed in the others. The contribution of thermal energy caused an increase of $C_{p,m}$ with T (Fig. 4a). The relationship was a linear equation and the coefficients are listed in Table 7. Estimated values of this property were obtained with the correlation of Taherzadeh (section 3.2) and compared with the ours (Fig. S4). The mean relative deviations were lower than 5 %. The Joule-Thomson coefficient (μ_{JT}) is a parameter of interest in industrial processes that expresses the variation in temperature with pressure changes at constant enthalpy. It can be calculated from $C_{p,m}$ and ρ values at different T as follows:

$$\mu_{JT} = \frac{V_m}{C_{p,m}}\left(T\cdot\alpha_p - 1\right), \tag{24}$$

The calculated μ_{JT} were negatives in the range of T studied. The absolute values as well as the difference between the μ_{JT} of the OA ESs decreased with increasing T (Table 5, Fig. 4b). Both thermodynamic properties were predicted with PC-SAFT EoS (section 3.1) and compared with those obtained in this work from experimental measurements. The results are found in Table 6 and Fig. S3c, and S3d, and the averages of the mean relative deviations were $MRD(C_{p,m})$=3.3 % and $MRD(\mu_{JT})$=1.9 %.

4.3. Surface tension

Moving a molecule from the bulk of the liquid to the air-liquid interface requires the contribution of energy needed to overcome the cohesive forces. The γ is a measure of this energy. The measured values were higher in those mixtures with aromatic components, showing that the intermolecular interactions are stronger (Tables 5 and S6). The γ of the mixtures with Oa was approximately 2 mN·m^{-1} higher than that of the mixtures with decanoic acid. This result would correspond to better structuring in the former as a result of the presence of more interactions. On the other hand, they weaken with thermal agitation so the slope of the $\gamma - T$ linear equation was negative (Table 7, Fig. 5a). From it, the entropy ($\Delta S_s = -(\partial\gamma/\partial T)_p$) and enthalpy ($\Delta H_S = \gamma - T(\partial\gamma/\partial T)_p$) of the surface per unit area were calculated (Table 5). The ΔS_s values for the mixtures with T and E were similar and lower than those of the other mixtures. The highest value was obtained for the least structured

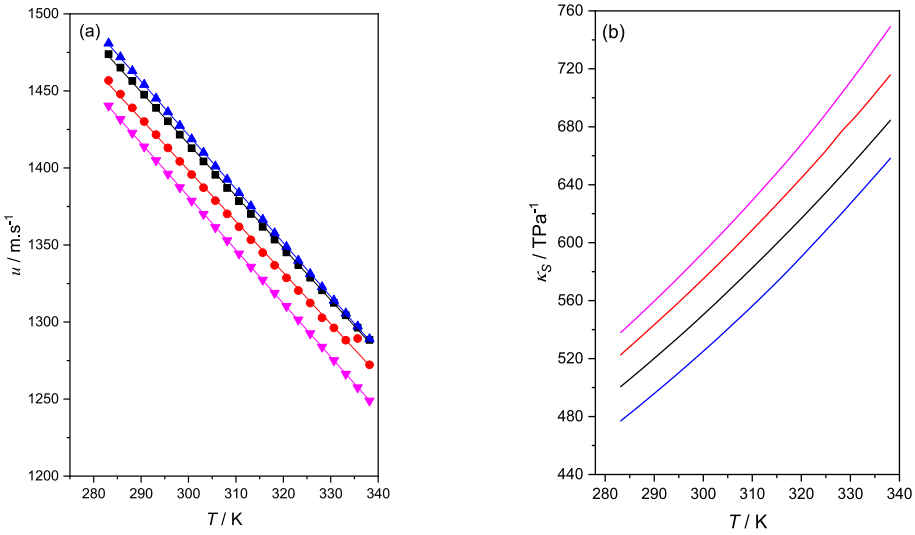

Fig. 2. Properties of oleic acid-based ESs at p=0.1 MPa at various temperatures (T) and compositions. (a), Speed of sound (u); (b) Isentropic compressibility, (κ_S). (■), Thymol:oleic acid, x_{Oa}=0.6; (●), l-menthol:oleic acid, x_{Oa}=0.5; (▲), eugenol:oleic acid, x_{Oa}=0.5; (▼), linalool:oleic acid, x_{Oa}=0.5. Points, experimental values; lines, calculated data.

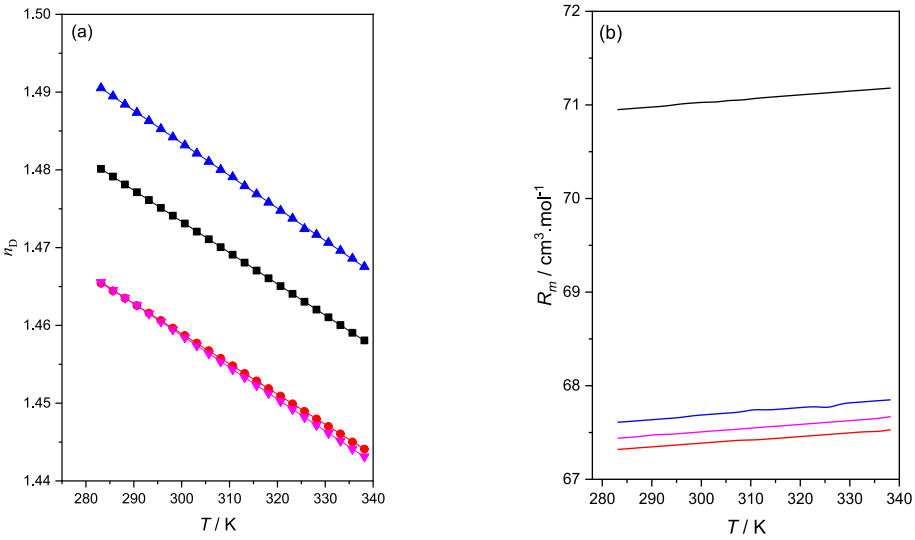

Fig. 3. Properties of oleic acid-based ESs at p=0.1 MPa at various temperatures (T) and compositions. (a), Refraction index (n_D); (b) Molar refraction (R_m). (■), Thymol:oleic acid, x_{Oa}=0.6; (●), l-menthol:oleic acid, x_{Oa}=0.5; (▲), eugenol:oleic acid, x_{Oa}=0.5; (▼), linalool:oleic acid, x_{Oa}=0.5. Points, experimental values; lines, calculated data.

mixture. Regarding ΔH_S, the values were similar for all mixtures and almost constant with T. Furthermore, increasing interface surface area causes a change in the fluid polarity so the γ and n_D are related. We used the Papazian equation (section 3.4). The linearity obtained is shown in Table 8 and Fig. 5b.

Many liquids undergo thermal decomposition before reaching the critical temperature (T_c), so this value is often impossible to determine experimentally. Nevertheless, these values are essential in the application of the thermodynamic models. To address this, group contribution methods are often used in the literature. Here, we calculated them using the Guggenheim and Eotvos equations (section 3.3), considering that γ tends to zero as the fluid approaches at the critical point. We have also estimated T_c and the critical pressure (p_c) using the Lee-Kesler method (section 3.2) and the PC-SAFT EoS (section 3.1). Tables 9 and 10 present the values obtained with the four methods. The data calculated for each Oa ESs with the EoS were the lowest. Fig. 6 display the critical loci estimated of the four systems.

4.3.1. *Viscosity*

The fluidity of a solvent can be a determining factor in the efficiency of a process, especially when mass transfer is involved. This property is indicative of the resistance to movement due to friction between the layers of the liquid. It depends both on the size and shape of the molecules and on the interactions between them. The η measured in this work were moderate, well below the 100 mPa·s, value established as the maximum for good solvent performance (Van Osch et al., 2019). They ranged from 4.79 mPa·s for LOa at 338.15 K to 69.25 mPa·s for MOa at 283.15 K, and the sequence was LOa < EOa < T3Oa5 < MOa (Tables 4 and S7). This property is greatly influenced by the shape of the molecules involved. Thus, the mixtures studied here had close to three times the viscosity of the corresponding mixtures containing decanoic acid. This is consistent with the well-known steric hindrance that Oa presents to the movement of molecules between layers. The influence of T on transport properties as η is more pronounced at lower T, so the relationship is exponential as seen in Fig. 7a. We used the VFT equation with

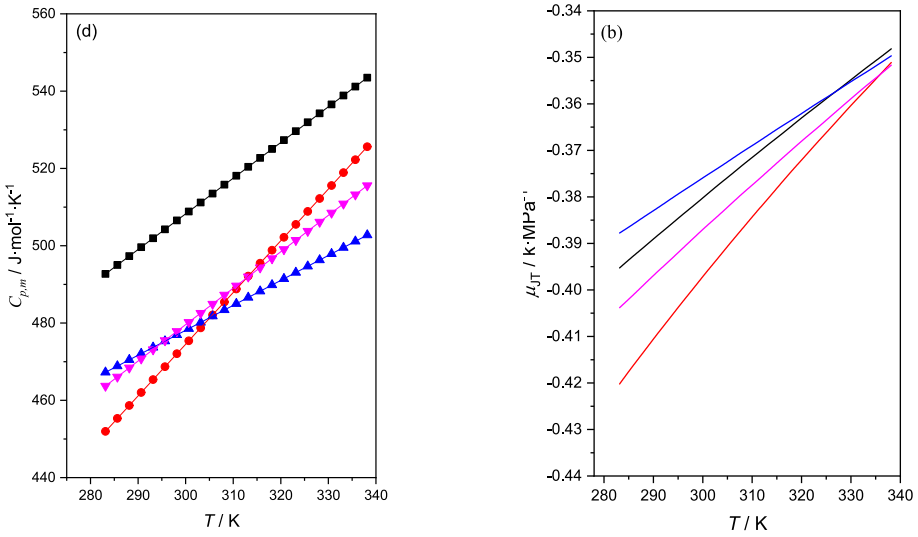

Fig. 4. Properties of oleic acid-based ESs at p=0.1 MPa at various temperatures (T) and compositions. (a), Isobaric molar heat capacity ($C_{p,m}$); (b) Joule-Thomson coefficient (μ_{JT}). (■), Thymol:oleic acid, x_{Oa}=0.6; (●), l-menthol:oleic acid, x_{Oa}=0.5; (▲), eugenol:oleic acid, x_{Oa}=0.5; (▼), linalool:oleic acid, x_{Oa}=0.5. Points, experimental values; lines, calculated data.

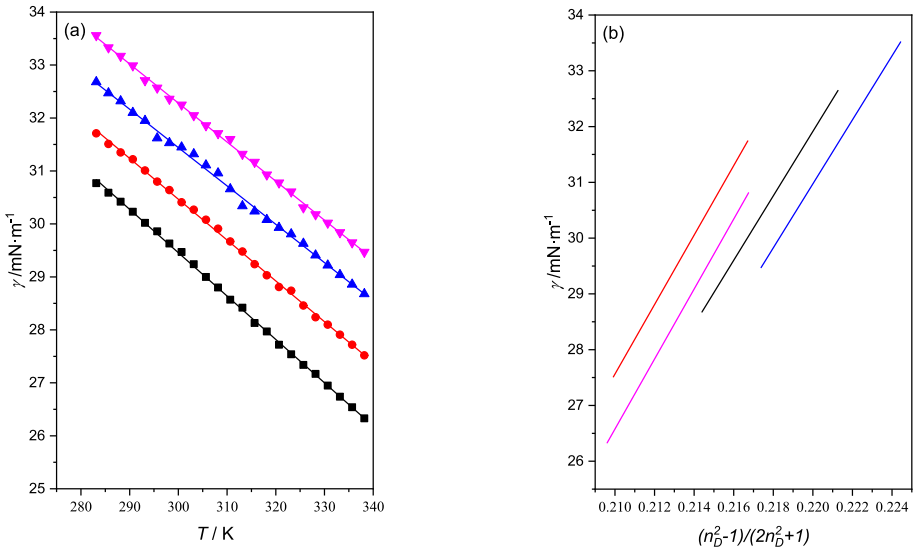

Fig. 5. (a), Surface tension (γ) of oleic acid-based ESs at p=0.1 MPa, at various temperatures (T) and compositions. (b) Papazian correlation (eq. 20). (■), Thymol:oleic acid, x_{Oa}=0.6; (●), l-menthol:oleic acid, x_{Oa}=0.5; (▲), eugenol:oleic acid, x_{Oa}=0.5; (▼), linalool:oleic acid, x_{Oa}=0.5. Points, experimental values; lines, calculated data.

Table 8
Fit parameters of the surface tension correlations of the Oa ESs studied.

Equation	Parameter	T3Oa5[a]	MOa[b]	EOa[c]	LOa[d]
Papazian[e]	A	577.84	622.81	573.75	627.36
	B	−95.21	−103.22	−95.25	−105.17
	R^2	0.9972	0.9992	0.9993	0.9996
Pelofsky[f]	lnA_1	3.492	3.458	3.523	3.442
	B_1 / mPa·s	−0.971	−1.05	−0.789	−0.873
	R^2	0.97	0.97	0.98	0.98
Murkerjee[g]	lnA_2	3.247	3.208	3.282	3.153
	B_2/3	0.062	0.061	0.066	0.082
	R^2	0.98	0.98	0.98	0.98

[a] Thymol:oleic acid, x_{Oa}=0.6; [b] l-menthol:oleic acid, x_{Oa}=0.5; [c] eugenol:oleic acid, x_{Oa}=0.5; [d] linalool:oleic acid, x_{Oa}=0.5. [e] Eq. 20; [f] Eq. 21; [g] (22)

Table 9
Estimation of the critical temperatures (T_c) and pressures (p_c) of the Oa ESs studied.

Oa ESs	Lee-Kesler[e]		Guggenheim[f]	Eötvos[g]
	T_c/K	p_c/MPa	T_c/K	T_c/K
T3Oa5[a]	845.16	1.75	856.68	856.67
MOa[b]	787.19	1.76	809.49	792.78
EOa[c]	826.77	1.84	861.14	865.70
LOa[d]	777.85	1.76	764.81	743.90

[a] Thymol:oleic acid, x_{Oa}=0.6; [b] l-menthol:oleic acid, x_{Oa}=0.5; [c] eugenol:oleic acid, x_{Oa}=0.5; [d] linalool:oleic acid, x_{Oa}=0.5. [e] Eq. 12–17; [f] Eq. 18; [g] (19)

Table 10
Prediction from PC-SAFT EoS (eq. 1–9) of the critical temperatures (T_c) and critical pressures (p_c) of the systems studied at different mole fractions of oleic acid (x_{Oa}). k_{ij}=0.

	Thymol:Oleic Acid		l-menthol:Oleic Acid		Eugenol:Oleic Acid		Linalool:Oleic Acid	
x_{Oa}	T_c/K	p_c/MPa	T_c/K	p_c/MPa	T_c/K	p_c/MPa	T_c/K	p_c/MPa
0	734.1	3.81	693.0	3.31	755.6	3.82	678.5	2.97
0.1	743.9	3.55	709.4	3.24	760.6	3.50	703.6/ 719.6 [a]	3.06/ 3.28 [a]
0.2	752.4	3.29	724.0	3.11	765.6	3.21	722.6/ 743.2 [a]	2.99/ 3.16 [a]
0.3	760.4	3.03	736.9	2.94	770.3	2.94	737.8/ 758.6 [a]	2.84/ 2.92 [a]
0.4	767.1	2.78	748.4	2.75	774.7	2.71	750.1/ 769.3 [a]	2.67/ 2.68 [a]
0.5	773.0	2.55	758.4	2.55	778.6	2.48	760.4/ 776.9 [a]	2.48/ 2.45 [a]
0.6	778.2	2.33	767.2	2.35	782.3	2.28	769.2/ 782.6 [a]	2.30/ 2.25 [a]
0.7	782.8	2.14	775.1	2.16	785.6	2.10	776.7/ 786.8 [a]	2.11/ 2.06 [a]
0.8	787.0	1.95	782.2	1.97	788.7	1.93	783.3/ 790.0 [a]	1.94/ 1.90 [a]
0.9	790.8	1.79	788.5	1.80	791.6	1.77	789.0/ 792.4[a]	1.78/ 1.76 [a]
1	794.2	1.63	794.2	1.63	794.2	1.63	794.2	1.63

[a] k_{ij}= −0.05.

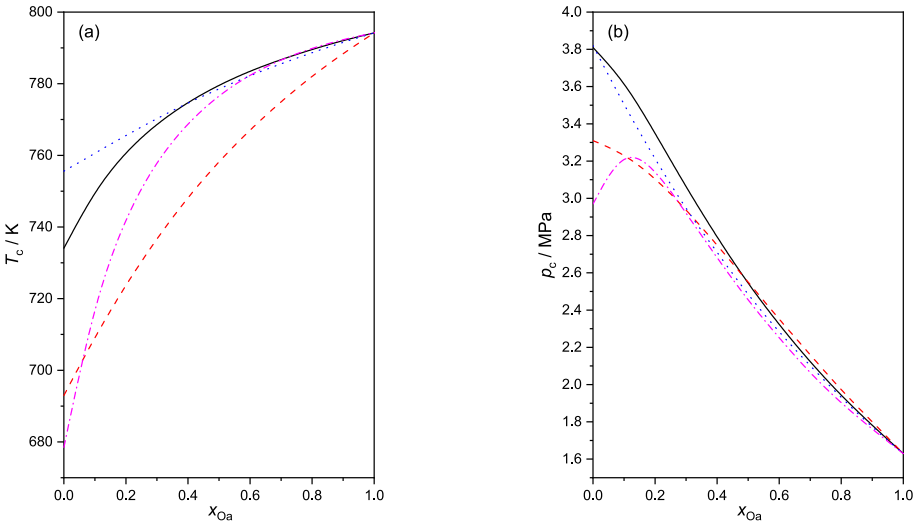

Fig. 6. PC-SAFT estimation of the critical loci of oleic acid-based ESs. (a) Critical temperature (T_c); (b), Critical pressure (p_c). (—), Thymol:oleic acid, x_{Oa}=0.6, k_{ij}= 0; (— —), l-menthol:oleic acid, x_{Oa}=0.5, k_{ij}=0; (· · ·), eugenol:oleic acid, x_{Oa}=0.5, k_{ij}=0; (— · –), linalool:oleic acid, x_{Oa}=0.5, k_{ij}= −0.05.

three parameters (A, B, C). Parameter A indicates the contribution to viscosity due solely to the steric issues and the others are related to the interactions to be overcome between layers. The latter is the activation energy of viscosity flow ($E_{a,\eta}$) calculated as $E_{a,\eta} = R(\partial \ln\eta / \partial(1/T))$. The equation expression and parameter values are listed in Table 11. The similarity of the trend of η and $E_{a,\eta}$with T shows that interactions influenced viscosity more than steric issues (Fig. 7a and 7b). An increase in the surface area of the interface also implies the movement of molecules between the fluid layers. Therefore, it is logical that γ and η are related. In this work, the relationships used were those proposed by Pelofsky and Murkerjee (section 3.4) whose parameters are found in Table 8. A high linearity was obtained in both cases with regression coefficients greater than 0.97.

5. Conclusions

This work presents the characterization of four binary eutectic mixtures composed by oleic acid (Oa) and thymol (T), or l-menthol (M), or eugenol (E), or linalool (L). Hydrophobic eutectic solvents, such as these mixtures, have proven to be a viable alternative in the extraction of natural products and in the solubilization of drugs and nutraceuticals that are poorly soluble in the aqueous phase. The composition of the mixtures was equimolar except for the one with T whose molar fraction was x_{Oa}=0.6. The following properties were measured at 0.1 MPa and from 283.15 to 338.15 K in intervals of 2.5 K: density, speed of sound, refractive index, isobaric molar heat capacity, surface tension, and viscosity. From them, different properties were calculated and correlations were applied. Furthermore, the PC-SAFT equation of state (EoS) was validated for these systems. From phase change data, it can be concluded that the mixtures with T and M were slightly eutectic, and those with E and L showed ideal behavior. Except for $C_{p,m}$ and η, the trend found for the rest of the properties was LOa < MOa < T3Oa5 < EOa. This result showed that the most compact and structured mixtures were those containing an aromatic ring in the structure. The $C_{p,m}$ value was similar

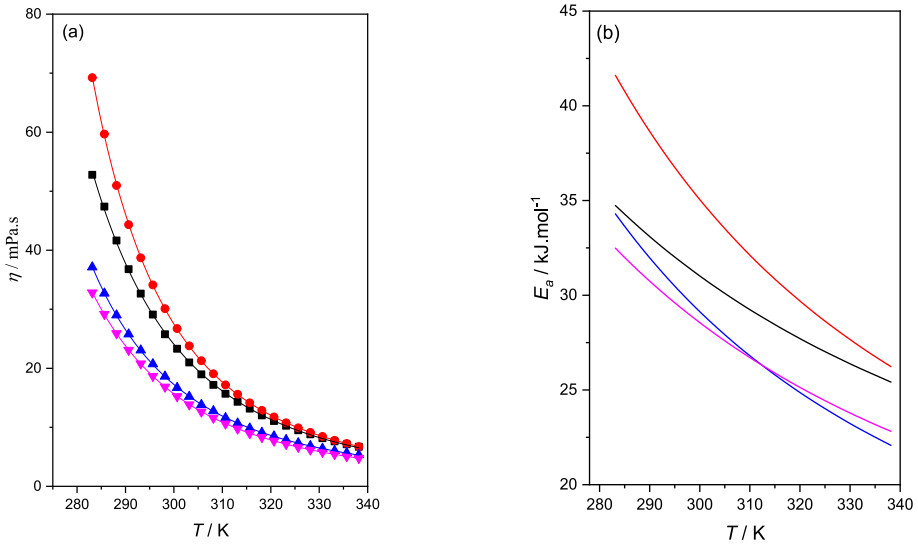

Fig. 7. Properties of oleic acid-based ESs at p=0.1 MPa at various temperatures (T) and compositions. (a), Dynamic viscosity (η); (b) Activation energy for viscous flow, ($E_{a,\eta}$). (■), Thymol:oleic acid, x_{Oa}=0.6; (●), l-menthol:oleic acid, x_{Oa}=0.5; (▲), eugenol:oleic acid, x_{Oa}=0.5; (▼), linalool:oleic acid, x_{Oa}=0.5. Points, experimental values; lines, calculated data.

Table 11
Correlation of the dynamic viscosity with temperature, VFT equation [a], of the Oa ESs studied. Fitting parameters (A, B, C) and regression coefficients (R^2).

Oa ESs	A	B	C	R^2
T3Oa5[b]	0.02809	1078.77	140.28	0.9997
MOa[c]	0.06076	784.65	171.70	0.9999
EOa[d]	0.08758	701.72	167.20	0.9999
LOa[e]	0.04464	880.37	149.82	0.9999

[a] $\eta = A\exp\left[\frac{B}{T-C}\right]$, [b] Thymol:oleic acid, x_{Oa}=0.6; [c] l-menthol:oleic acid, x_{Oa}=0.5; [d] eugenol:oleic acid, x_{Oa}=0.5; [e] linalool:oleic acid, x_{Oa}=0.5.

for the equimolar mixtures, around 470 J/mol·K, and it was about 30 J/mol·K higher for the mixture with T due to its higher Oa content. For all mixtures, the value of the Joule-Thomson coefficient was within (-0.4 ± 0.01) K/MPa. The deviations between $C_{p,m}$ values measured and those obtained with the Taherzadeh correlation were less than 5 %. A very high linearity (R^2>0.997) was found in the $\gamma - n_D$ correlation. Moreover, the mixture containing the acyclic compound (LOa) was the most fluid and MOa was the most viscous. The γ was also well correlated with η and the regression coefficients were greater than 0.97. Finally, the PC-SAFT adequately predicted the volumetric and calorific properties.

CRediT authorship contribution statement

Elena Pérez-Pueyo: Resources, Investigation, Data curation. **Héctor Artigas:** Validation, Methodology. **Mohammadreza Haftbaradaran Esfahani:** Data curation. **Carlos Lafuente:** Writing – original draft, Project administration, Methodology. **Manuela Artal:** Writing – review & editing, Writing – original draft, Conceptualization.

Declaration of competing interest

The authors declare that they have no known competing financial interests or personal relationships that could have influenced the work reported in this paper.

Acknowledgments

PLATON research group acknowledges financial support from Gobierno de Aragón and Fondo Social Europeo "Construyendo Europa desde Aragón" _E31_23R. The authors would like to thank Dr. Ignacio Delso (School of Chemistry, Pharmacy and Pharmacology, University of East Anglia, Norwich, United Kingdom) and the Center for Chemistry and Materials of Aragon (CEQMA, University of Zaragoza) for their collaboration in the resolution of the NMR spectra.

Appendix A. Supplementary data

Supplementary data to this article can be found online at https://doi.org/10.1016/j.foodres.2025.117802.

Data availability

The authors confirm that the data supporting the findings of this study are available within the article and its supplementary materials

References

Abdelquader, M. M., Li, S., Andrews, G. P., & Jones, D. S. (2023). Therapeutic deep eutectic solvents: A comprehensive review of their thermodynamics, microstructure and drug delivery applications. *European Journal of Pharmaceutics and Biopharmaceutics, 186*(February), 85–104. https://doi.org/10.1016/j.ejpb.2023.03.002

Abranches, D. O., Martins, M. A. R., Silva, L. P., Schaeffer, N., Pinho, S. P., & Coutinho, J. A. P. (2019). Phenolic hydrogen bond donors in the formation of non-ionic deep eutectic solvents: The quest for type V DES. *Chemical Communications, 55*(69), 10253–10256. https://doi.org/10.1039/C9CC04846D

An, Q., Ren, J.-N., Li, X., Fan, G., Qu, S.-S., Song, Y., Li, Y., & Pan, S.-Y. (2021). Recent updates on bioactive properties of linalool. *Food & Function, 12*(21), 10370–10389. https://doi.org/10.1039/D1FO02120F

Antón, V., Artigas, H., Muñoz-Embid, J., Artal, M., & Lafuente, C. (2017). Thermophysical study of 2-acetylthiophene: Experimental and modelled results. *Fluid Phase Equilibria, 433*, 126–134. https://doi.org/10.1016/j.fluid.2016.10.026

Artigas-Hernández, D., Berzosa, A., Aguilar-Machado, D., Raso, J., & Artal, M. (2023). Using eutectic solvents for extracting astaxanthin from dry biomass of Xanthophyllomyces dendrorhous pretreated by pulsed electric fields. *Separation and Purification Technology, 324*(April). https://doi.org/10.1016/j.seppur.2023.124496

Bergua, F., Castro, M., Lafuente, C., & Artal, M. (2022). Thymol+l-menthol eutectic mixtures: Thermophysical properties and possible applications as decontaminants. *Journal of Molecular Liquids, 368*, Article 120789. https://doi.org/10.1016/j.molliq.2022.120789

Bergua, F., Castro, M., Muñoz-Embid, J., Lafuente, C., & Artal, M. (2021). Hydrophobic eutectic solvents: Thermophysical study and application in removal of

pharmaceutical products from water. *Chemical Engineering Journal, 411*(January). https://doi.org/10.1016/j.cej.2021.128472
Bergua, F., Castro, M., Muñoz-Embid, J., Lafuente, C., & Artal, M. (2022). L-menthol-based eutectic solvents: Characterization and application in the removal of drugs from water. *Journal of Molecular Liquids, 352*, Article 118754. https://doi.org/10.1016/j.molliq.2022.118754
Bergua, F., Delso, I., Muñoz-Embid, J., Lafuente, C., & Artal, M. (2021). Structure and properties of two glucose-based deep eutectic systems. *Food Chemistry, 336*(July 2020), Article 127717. https://doi.org/10.1016/j.foodchem.2020.127717
Brocos, P., Piñeiro, Á., Bravo, R., & Amigo, A. (2003). Refractive indices, molar volumes and molar refractions of binary liquid mixtures: Concepts and correlations. *Physical Chemistry Chemical Physics, 5*(3), 550–557. https://doi.org/10.1039/b208765k
Chen, C., He, L., Tian, Y., & Xie, J. (2025). Improving the preparation process to enhance the retention of cinnamon essential oil in thermoplastic starch/PBAT active film and its antimicrobial activity. *Industrial Crops and Products, 230*, Article 120990. https://doi.org/10.1016/j.indcrop.2025.120990
Corvis, Y., & Espeau, P. (2012). Incidence of chirality on the properties of mixtures containing an amide type anesthetic compound. *Thermochimica Acta, 539*, 39–43. https://doi.org/10.1016/j.tca.2012.03.027
Delso, I., Lafuente, C., Muñoz-Embid, J., & Artal, M. (2019). NMR study of choline chloride-based deep eutectic solvents. *Journal of Molecular Liquids, 290*, Article 111236. https://doi.org/10.1016/j.molliq.2019.111236
Duque, A., Sanjuan, A., Bou-Ali, M. M., Alonso, R. M., & Campanero, M. A. (2023). Physicochemical characterization of hydrophobic type III and type V deep eutectic solvents based on carboxylic acids. *Journal of Molecular Liquids, 392*(P1), Article 123431. https://doi.org/10.1016/j.molliq.2023.123431
Ferreira, C., & Sarraguça, M. (2024). *A comprehensive review on deep eutectic solvents and its use to extract bioactive compounds of pharmaceutical interest. In pharmaceuticals (Vol. 17, issue 1)*. Multidisciplinary digital publishing institute (MDPI). https://doi.org/10.3390/ph17010124
García-Zapateiro, L. A., Franco, J. M., Valencia, C., Delgado, M. A., & Gallegos, C. (2013). Viscous, thermal and tribological characterization of oleic and ricinoleic acids-derived estolides and their blends with vegetable oils. *Journal of Industrial and Engineering Chemistry, 19*(4), 1289–1298. https://doi.org/10.1016/j.jiec.2012.12.030
Gross, J., & Sadowski, G. (2000). Application of perturbation theory to a hard-chain reference fluid: An equation of state for square-well chains. *Fluid Phase Equilibria, 168*(2), 183–199. https://doi.org/10.1016/S0378-3812(00)00302-2
Gross, J., & Sadowski, G. (2001). Perturbed-chain SAFT: An equation of state based on a perturbation theory for chain molecules. *Industrial and Engineering Chemistry Research, 40*(4), 1244–1260. https://doi.org/10.1021/ie0003887
Guggenheim, E. A. (1945). The principle of corresponding states. *Journal of Physical Chemistry, 13*, 253–261.
Ion, S., Olănescu, F., Teodorescu, F., Tincu, R., Gheorghe, D., Pârvulescu, V. I., & Tudorache, M. (2022). DES-based biocatalysis as a green alternative for the l-menthyl Ester production based on l-menthol acylation. *Molecules, 27*(16), 5273. https://doi.org/10.3390/molecules27165273
Isci, A., & Kaltschmitt, M. (2022). Recovery and recycling of deep eutectic solvents in biomass conversions: a review. In *, Vol. 12. Biomass conversion and biorefinery* (pp. 197–226). Springer Science and Business Media Deutschland GmbH. https://doi.org/10.1007/s13399-021-01860-9.
Jacobson, B. (1952). Ultrasonic velocity in liquids and liquid mixtures. *The Journal of Chemical Physics, 20*(5), 927–928. https://doi.org/10.1063/1.1700615
Khwaza, V., & Aderibigbe, B. A. (2025). Antibacterial activity of selected essential oil components and their derivatives: A review. *Antibiotics, 14*(1), 68. https://doi.org/10.3390/antibiotics14010068
Liu, Y., Friesen, J. B., McAlpine, J. B., Lankin, D. C., Chen, S. N., & Pauli, G. F. (2018). Natural deep eutectic solvents: Properties, applications, and perspectives. *Journal of Natural Products, 81*(3), 679–690. https://doi.org/10.1021/acs.jnatprod.7b00945
López, N., Delso, I., Matute, D., Lafuente, C., & Artal, M. (2020). Characterization of xylitol or citric acid:Choline chloride:Water mixtures: Structure, thermophysical properties, and quercetin solubility. *Food Chemistry, 306*. https://doi.org/10.1016/j.foodchem.2019.125610
del Mar Contreras-Gámez, M., Galán-Martín, Á., Seixas, N., da Costa Lopes, A. M., Silvestre, A., & Castro, E. (2023). Deep eutectic solvents for improved biomass pretreatment: Current status and future prospective towards sustainable processes. In *, Vol. 369. Bioresource technology*. Elsevier Ltd.. https://doi.org/10.1016/j.biortech.2022.128396
Marañés, J., Berzosa, A., Bergua, F., Marín-Sánchez, J., Raso, J., & Artal, M. (2025). Eutectic mixtures based on oleic acid and pulsed electric fields: A strategy for the extraction of Astaxanthin from dry biomass of Xanthophyllomyces dendrorhous. *Foods, 14*(13), 2371. https://doi.org/10.3390/foods14132371
Martins, M. A. R., Crespo, E. A., Pontes, P. V. A., Silva, L. P., Bülow, M., Maximo, G. J., Batista, E. A. C., Held, C., Pinho, S. P., & Coutinho, J. A. P. (2018). Tunable hydrophobic eutectic solvents based on terpenes and monocarboxylic acids. *ACS Sustainable Chemistry and Engineering, 6*(7), 8836–8846. https://doi.org/10.1021/acssuschemeng.8b01203
Martins, M. A. R., Pinho, S. P., & Coutinho, J. A. P. (2018). Insights into the nature of eutectic and deep eutectic mixtures. *Journal of Solution Chemistry, August.*. https://doi.org/10.1007/s10953-018-0793-1
Mussagy, C. U., Farias, F. O., Sasaki, J. C., Scontri, M., Picheli, F., Santos-Ebinuma, V. C., de Azeredo, H. M. C., Pessoa, A., & Herculano, R. D. (2023). Eutectic solvent-based bioactive films functionalized with microbial astaxanthin extends shelf life of fresh strawberries. *Materials Today Chemistry, 33*. https://doi.org/10.1016/j.mtchem.2023.101721
Mussagy, C. U., Remonatto, D., Picheli, F. P., Paula, A. V., Herculano, R. D., Santos-Ebinuma, V. C., Farias, R. L., Onishi, S. D., & B., J. L. Ribeiro, S., F. B. Pereira, J., & Pessoa, A. (2022). A look into Phaffia rhodozyma biorefinery: From the recovery and fractionation of carotenoids, lipids and proteins to the sustainable manufacturing of biologically active bioplastics. *Bioresource Technology, 362*. https://doi.org/10.1016/j.biortech.2022.127785
Mussagy, C. U., Santos-Ebinuma, V. C., Herculano, R. D., Coutinho, J. A. P., Pereira, J. F. B., & Pessoa, A. (2022). Ionic liquids or eutectic solvents? Identifying the best solvents for the extraction of astaxanthin and β-carotene from Phaffia rhodozyma yeast and preparation of biodegradable films. *Green Chemistry, 24*(1), 118–123. https://doi.org/10.1039/d1gc03521e
Padilla, N., Delso, I., Bergua, F., Lafuente, C., & Artal, M. (2024). Characterization of camphor: Thymol or dl-menthol eutectic mixtures; structure, thermophysical properties, and lidocaine solubility. *Journal of Molecular Liquids, 405*. https://doi.org/10.1016/j.molliq.2024.125069
Paiva, A., Craveiro, R., Aroso, I., Martins, M., Reis, R. L., Barreiros, S., & Duarte, A. R. C. (2014). Natural deep eutectic solvents-solvents for the 21st century. *ACS Sustainable Chemistry and Engineering, 2*, 1063–1071. https://doi.org/10.1021/sc500096j
Papazian, H. A. (1971). Correlation of surface tension between various liquids. *Journal of the American Chemical Society, 93*(22), 5634–5636. https://doi.org/10.1021/ja00751a008
Pelofsky, A. H. (1966). Surface tension-viscosity relation for liquids. *Journal of Chemical and Engineering Data, 11*(3), 394–397. https://doi.org/10.1021/je60030a031
Pitacco, W., Samorì, C., Pezzolesi, L., Gori, V., Grillo, A., Tiecco, M., Vagnoni, M., & Galletti, P. (2022). Extraction of astaxanthin from Haematococcus pluvialis with hydrophobic deep eutectic solvents based on oleic acid. *Food Chemistry, 379*. https://doi.org/10.1016/j.foodchem.2022.132156
Pour, S. B., Sardroodi, J. J., & Ebrahimzadeh, A. R. (2022). Structure and dynamics of thymol - fatty acids based deep eutectic solvent investigated by molecular dynamics simulation. *Fluid Phase Equilibria, 552*, Article 113241. https://doi.org/10.1016/j.fluid.2021.113241
Prausnitz, J. M., Lichtenthaler, R. N., & Azevedo, E. G. (1986). *Molecular thermodynamics of the fluid phase equilibria*. Prentice-Hall.
Radwan, I. T., El-Sherbiny, I. M., & Metwally, N. H. (2024). Synergistic and potential antifungal properties of tailored, one pot multicomponent monoterpenes co-delivered with fluconazole encapsulated nanostructure lipid carrier. *Scientific Reports, 14*(1), 14382. https://doi.org/10.1038/s41598-024-63149-x
dos Santos, P. R. S., Voll, F. A. P., Ramos, L. P., & Corazza, M. L. (2017). Esterification of fatty acids with supercritical ethanol in a continuous tubular reactor. *The Journal of Supercritical Fluids, 126*, 25–36. https://doi.org/10.1016/j.supflu.2017.03.002
Shereshefsky, J. L. L. (1930). Surface tension of saturated vapors and the equation of Eötvos. *Journal of Physical Chemistry, 35*(6), 1712–1720. https://doi.org/10.1021/j150324a014
Sieniawska, E., Swatko-Ossor, M., Sawicki, R., Skalicka-Woźniak, K., & Ginalska, G. (2017). Natural terpenes influence the activity of antibiotics against isolated mycobacterium tuberculosis. *Medical Principles and Practice, 26*(2), 108–112. https://doi.org/10.1159/000454680
Sportiello, L., Favati, F., Condelli, N., Di Cairano, M., Caruso, M. C., Simonato, B., Tolve, R., & Galgano, F. (2023). Hydrophobic deep eutectic solvents in the food sector: Focus on their use for the extraction of bioactive compounds. In *, Vol. 405. Food chemistry*. Elsevier Ltd.. https://doi.org/10.1016/j.foodchem.2022.134703
Štejfa, V., Bazyleva, A., Fulem, M., Rohlíček, J., Skořepová, E., Růžička, K., & Blokhin, A. V. (2019). Polymorphism and thermophysical properties of l- and dl-menthol. *The Journal of Chemical Thermodynamics, 131*, 524–543. https://doi.org/10.1016/j.jct.2018.11.004
Taherzadeh, M., Haghbakhsh, R., Duarte, A. R. C., & Raeissi, S. (2020). Estimation of the heat capacities of deep eutectic solvents. *Journal of Molecular Liquids, 307*, Article 112940. https://doi.org/10.1016/j.molliq.2020.112940
Tandon, P., Förster, G., Neubert, R., & Wartewig, S. (2000). Phase transitions in oleic acid as studied by X-ray diffraction and FT-Raman spectroscopy. *Journal of Molecular Structure, 524*(1), 201–215. https://doi.org/10.1016/S0022-2860(00)00378-1
Tapia-Quirós, P., Granados, M., Sentellas, S., & Saurina, J. (2024). Microwave-assisted extraction with natural deep eutectic solvents for polyphenol recovery from agrifood waste: Mature for scaling-up?. In *, Vol. 912. Science of the Total environment*. Elsevier B.V. https://doi.org/10.1016/j.scitotenv.2023.168716.
Torcal, M., Teruel, M. I., García, J., Urieta, J. S., & Mainar, A. M. (2010). *P ρ T* measurements of the (ethanol + linalool), (Propan-1-ol + linalool), and (Propan-2-ol + linalool) mixtures: Cubic and statistical associating fluid theory-based equation of state analyses. *Journal of Chemical & Engineering Data, 55*(11), 5332–5339. https://doi.org/10.1021/je100581m
Van Osch, D. J. G. P., Dietz, C. H. J. T., Van Spronsen, J., Kroon, M. C., Gallucci, F., Van Sint Annaland, M., & Tuinier, R. (2019). A search for natural hydrophobic deep eutectic solvents based on natural components [research-article]. *ACS Sustainable Chemistry and Engineering, 7*(3), 2933–2942. https://doi.org/10.1021/acssuschemeng.8b03520
Van Osch, D. J. G. P., Zubeir, L. F., Van Den Bruinhorst, A., Rocha, M. A. A., & Kroon, M. C. (2015). Hydrophobic deep eutectic solvents as water-immiscible extractants. *Green Chemistry, 17*(9), 4518–4521. https://doi.org/10.1039/c5gc01451d
Vlacha, M., Giannakas, A., Katapodis, P., Stamatis, H., Ladavos, A., & Barkoula, N. M. (2016). On the efficiency of oleic acid as plasticizer of chitosan/clay nanocomposites and its role on thermo-mechanical, barrier and antimicrobial properties - comparison with glycerol. *Food Hydrocolloids, 57*, 10–19. https://doi.org/10.1016/j.foodhyd.2016.01.003
Wang, Y., Jin, J., Wu, G., Wei, W., Jin, Q., & Wang, X. (2024). Omega-9 monounsaturated fatty acids: a review of current scientific evidence of sources,

metabolism, benefits, recommended intake, and edible safety. In *Critical reviews in food science and nutrition*. Taylor and Francis Ltd.. https://doi.org/10.1080/10408398.2024.2313181

Yan, Y., Shen, L., Wang, Y., Gong, B., Li, Z., & Qiu, H. (2025). Development of switchable deep eutectic solvents: Applications in extraction of natural products. *Chinese Chemical Letters, 36*(11), Article 110845. https://doi.org/10.1016/j.cclet.2025.110845

Zhang, J., Yao, L., Li, S., Li, S., Wu, Y., Li, Z., & Qiu, H. (2023). Green materials with promising applications: Cyclodextrin-based deep eutectic supramolecular polymers. *Green Chemistry, 25*(11), 4180–4195. https://doi.org/10.1039/D3GC00489A

Zielińska-Błajet, M., Pietrusiak, P., & Feder-Kubis, J. (2021). Selected monocyclic monoterpenes and their derivatives as effective anticancer therapeutic agents. *International Journal of Molecular Sciences, 22*(9), 4763. https://doi.org/10.3390/ijms22094763